Generating Wind Time Series as a Hybrid of Measured and Simulated Data

Stephen Rose and Jay Apt
Carnegie Mellon Electricity Industry Center, Carnegie Mellon University, 5000 Forbes Avenue, Pittsburgh PA 15213

Abstract: Certain applications, such as analyzing the effect of a wind farm on grid frequency regulation, require several years of wind power data measured at intervals of a few seconds. We have developed a method to generate days to years of non-stationary wind speed time series sampled at high rates by combining measured and simulated data. Measured wind speed data, typically 10 - 15 minute averages, captures the non-stationary characteristics of wind speed variation: diurnal variations, the passing of weather fronts, and seasonal variations. Simulated wind speed data, generated from spectral models, adds realistic turbulence between the empirical data. The wind speed time series generated with this method agree very well with measured time series, both qualitatively and quantitatively. The power output of a wind turbine simulated with wind data generated by this method demonstrates energy production, ramp rates, and reserve requirements that closely match the power output of a turbine simulated turbine with measured wind data.

1. Introduction

Planning for frequency control in a power system with significant amounts of wind power requires both high-frequency data (~1 Hz) to capture fast changes in power output and long periods of data to capture diurnal and seasonal variations. Similarly, simulating the fatigue life of wind turbine mechanical components requires high-frequency data to capture the dynamic effects of control system actions, but long periods of data to compile statistical data to more accurately estimate lifetimes. In both cases, large amounts of data are needed to design systems that are neither overly conservative and inefficient nor unreliable.

Long wind speed data sets sampled at high rates are often difficult to obtain. Empirical data are often sampled at too slow a rate, in the wrong location, or at the wrong height. Government meteorological services record many years of wind speed data, but it is typically sampled at slow rates (2 minute moving average in the USA) with low amplitude resolution (1 knot, 0.51 m/s, in the USA) [1] and at locations that are not valuable for wind power development. Wind farm developers collect several years of data at potential wind power sites, but they typically record 10-15 minute average values that are sufficient to estimate only long-term power production. Special scientific campaigns sometimes collect weeks to years of high-frequency data, but there are few of them because they are expensive to set up and maintain. The measurement instruments on a wind turbine are one of the best sources of this type of data, but the measurements can be confounded by the effects of the turbine and other turbines nearby, and data are frequently not archived at high temporal resolution.

Simulated wind speed data can be created at very high sampling rates, in any location, and at any height desired. However, simulation of periods longer than a few hours is difficult because wind speed variations are non-stationary processes: their statistical properties change over time. Those properties change with time of day, with the passing of weather fronts, and with the seasons. Most methods for simulating long periods of wind speed data use separate models for the non-stationary variations over longer periods (e.g. hours to months) and the stationary variations over shorter periods (e.g. seconds to minutes).

Previous authors have proposed a variety of methods for simulating non-stationary wind speed time series longer than a few hours [2]. The simulation methods divide the variations into high-frequency (periods less than approximately 15 minutes) and low-frequency (periods greater than 15 minutes) ranges. One method, that we will refer to as the "spectral method", joins together separate spectral models for the high- and low-frequency ranges in the frequency domain [3,4] and generates time series using the Veers method [5]. The other class of methods, that we will refer to as the "parametric method", models the high-frequency range using a spectral model and the low-frequency range using a probability distribution [6,7,8] or an auto-regressive moving average (ARMA) model [9]. Short periods (~10 minutes) of high-frequency data are generated using the Veers method, blended together, and then superimposed on low-frequency time series data. Most authors blend together the short time series of high-frequency data using a window function such as the Hann function that reduces leakage of energy outside the range of simulated frequencies [6,10], but one author concatenates together the high-frequency time series without any windowing because discontinuities are smaller than the largest sample-to-sample variations in the blocks of simulated data [7].

Both methods of modeling the low-frequency, non-stationary variations in wind speed are inadequate for certain types of power system planning and simulation because their simulations are not indexed to time of day and time of year. For example, the spectral and parametric methods can generate long time series that contain a certain level of wind speed variance with a

given probability, but those methods cannot model what time of day or time of year that level of variance is likely to occur. Electrical power demand is a relatively predictable function of time of day and time of year, so wind simulations must correctly model wind properties as a function of time. Nielsen addresses this problem in a non-stationary simulation of a wind front passage by specifying the statistical properties of wind turbulence at certain reference states, using Veers method to simulate stationary turbulence at those reference states, and then interpolating between the stationary simulations with Bezier curves fit to the reference states [11].

Our work addresses and solves the problem of correctly placing events in time by creating "hybrid" wind speed time series that combine measured low-frequency wind speed data with simulated high-frequency data. This hybrid method is similar to the parametric methods described above, especially Nielsen [11], but the hybrid method uses low-frequency measured wind speed data instead of the low-frequency data generated by parametric methods, and low-pass filtering of the measured data instead of windowing or interpolation. Low-frequency measured wind data is available from meteorological stations and meteorological towers at wind farms. Low-frequency wind speed data is also available from meso-scale simulations, but users should be very careful to understand the limitations of particular meso-scale models and the spatial and time resolutions of the data they generate.

Our work also improves on the procedure used in the parametric methods by filtering the low-frequency data to remove noise that leaks into the high-frequency region. This filtering fixes the problem of spurious low-frequency content in the Power Spectral Density (PSD) of data generated by McFarlane's method [6].

We demonstrate that this hybrid method creates wind time series that closely match the high-frequency and low-frequency characteristics of measured wind data and that the results of wind turbine simulations run with our hybrid wind closely match the results of turbine simulations run with measured wind data.

2. Hybrid Method for Generating Wind Data

We propose a hybrid method to generate long periods (days to years) of wind speed time series data by combining measured wind speed statistics sampled at low rates with simulated wind turbulence sampled at high rates. Measured statistics capture the non-stationary properties of real wind and simulated turbulence interpolates between the measured data. The hybrid method simulates short periods of turbulence using measured mean wind speed (and variance, if available) as a parameter, then superimposes the simulated turbulence on measured mean wind speed.

We define T as the total length of the period covered by the input data (in seconds); the total length of the output data is also T because the hybrid method interpolates the measured data. The sampling interval of the low-rate measured statistics is $T_{sample,\ input} = \frac{1}{f_{sample,\ input}}$ (in this paper, $T_{sample,input}$ = 600 seconds, $f_{sample,\ input}$ = 1.7 x 10^{-3} Hz). The sampling frequency of the output data is f_{output} (in this paper, f_{output} = 1 Hz).

A hybrid wind speed time series $u(t)$ of length T with output sampling frequency f_{output} is created by the following steps, illustrated in Figure 1:

A. Statistics of wind speed data are calculated over long intervals. In this paper, the wind speed mean and variance are measured with a sampling interval of $T_{sample,input}$ = 10 minutes.

B. A block of zero-mean, high-frequency turbulence is simulated for every *two* points of measured data ($2T_{sample,input}$) using a spectral model and the Veers method [5]. Blocks of turbulence are concatenated together without blending, overlapping, or windowing.

C. The measured mean wind speed is re-sampled to the desired sampling rate f_{output} and smoothed by a low-pass filter

D. The simulated turbulence is added to the smoothed mean to create the hybrid wind speed time series.

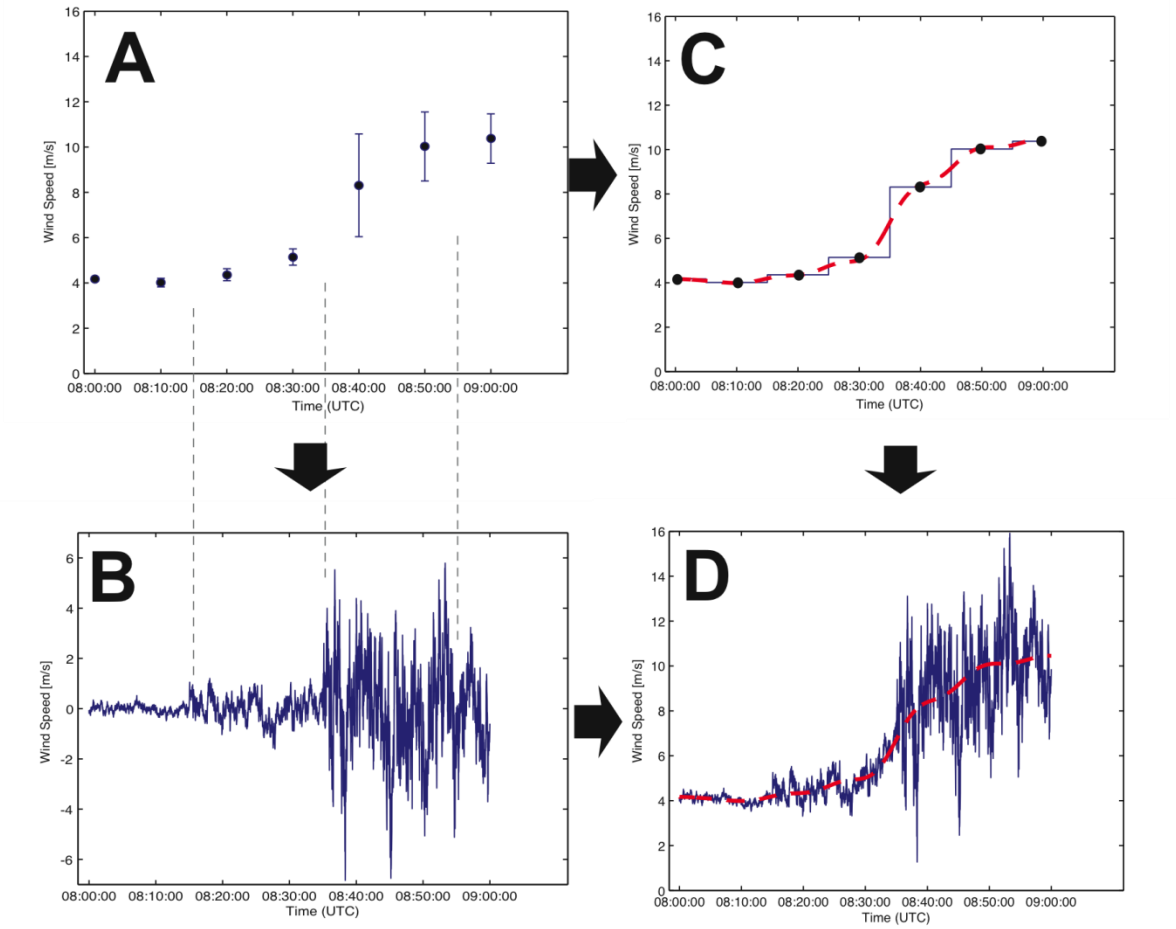

Figure 1: Procedure for generating wind speed time series from a hybrid of measured and simulated data. (A) Wind speed mean and variance measured for a long period T_{input} used as parameters to generate zero-mean turbulence in (B). The mean wind speeds in (A) are re-sampled at a higher rate f_{output} and smoothed by a low-pass filter in (C). The hybrid wind speed time series in (D) is the sum of (B) and (C).

2.1. Slowly-varying Measured Wind Speed (C)

The basis of a hybrid wind time series is mean wind speed measured at sampling intervals of $T_{sample,\ input}$. Low-rate mean wind speed captures slow changes such as diurnal and seasonal phenomena and the passing of weather fronts. Meteorological stations for wind resource assessment or weather prediction record the mean (and sometimes variance) of wind speed for periods of a few minutes. In this research, we use measured 10-minute mean $U_0(p)$ and variance $\sigma_u^2(p)$, where p is an index of the 10-minute period (Figure 1A).

We wish to create a time series of wind speeds of length T with a sampling rate of f_{output}. We re-sample the low-rate mean data to a sampling rate of f_{output} by repeating each measured mean

$U_0(p)$ at intervals f_{output} for a period of $T_{sample,\ input}$ (Figure 1C). Increasing the sampling rate from $f_{sample,input}$ to f_{output} does not add any new information, but it adds high-frequency noise. According to the sampling theorem, the maximum frequency signal that can be resolved by data sampled at $f_{sample,input}$ is $f_{Nyq,input} = \frac{1}{2T_{sample,input}}$ (the Nyquist frequency) [12]; all the content for frequencies higher than $f_{Nyq,\ input}$ is introduced noise. We remove the noise using a 3rd-order low-pass Butterworth filter with a cutoff frequency of $f_{cutoff} = f_{Nyq,input} = \frac{1}{2T_{input}}$, where the gain of the filter is $G = \left(1 + \left(\frac{f}{f_{cutoff}}\right)^6\right)^{-1/2}$. The low-pass filter is implemented in the frequency domain by applying the Fourier transform to the data, convolving the transformed data with the filter, and then applying the inverse Fourier transform. To avoid wrap-around effects from the Fourier transform, we de-trend the data by subtracting the best-fit line before applying the Fourier transform and then adding that best-fit line after applying the inverse Fourier transform.

2.2. High-rate Turbulence (B)

The hybrid method simulates high-rate turbulence to interpolate between measured mean wind speed values, shown in Figure 1B. For every two measured mean wind speeds $U_0(p)$ and $U_0(p+1)$, we generate a zero-mean turbulence time series of length $2T_{sample,\ input}$. To model the non-stationary properties of real wind, the variance of each simulated turbulence time series is a function of the corresponding measured mean wind speed (and variance, if available). We model wind turbulence with two variations of the Kaimal spectrum: the form given in Kaimal's original paper that models variance as a function of surface roughness length z_0 [13], and the form given in the IEC 61400-1 standard that takes wind speed variance as an explicit input [14].

Wind turbulence is simulated by a method developed by Shinozuka [15] and extended by Veers [5]. The Veers method simulates wind turbulence by taking the Fourier transform of a turbulence spectrum. The procedure for simulating wind turbulence by Veers method is described in detail in many other sources [3,5,16] and summarized here:

1. Define a 1-sided spectrum for the wind turbulence $S(f)$
2. Discretize the spectrum for the desired output period and sample rate: $S[m] = S(f)\Delta f$
3. Scale the discretized spectrum and apply random phase angles: $\mathbf{V}[m] = \sqrt{\frac{1}{2}\eta\, S[m]}\, e^{i\phi[m]}$
4. Construct a two-sided spectrum $\mathbf{V}_{2\ side}$
5. Calculate the turbulence time series: $\mathbf{u} = |\mathrm{FFT}(\mathbf{V}_{2\ side})|$

If the wind speed variance σ^2_u is known, the one-sided Kaimal spectral model specified in the IEC 61400-1 standard [14] can be used:

$$S(f) = \sigma_u^2 \frac{4\left(\frac{L_1}{U_0}\right)}{\left(1+6\left(\frac{L_1}{U_0}\right)f\right)^{5/3}} \quad (1)$$

If the wind speed variance is not known but the surface roughness length z_0 is known (or can be estimated), the one-sided Kaimal spectral model proposed by Kaimal [13] can be used:

$$S(f) = u_*^2 \frac{105\left(\frac{z}{U_0}\right)}{\left(1+33\left(\frac{z}{U_0}\right)f\right)^{5/3}} \quad (2)$$

where

σ_u = 10-minute standard deviation of longitudinal wind speed [m^2/s^2]

U_0 = 10-minute mean of longitudinal wind speed [m/s]

$$u_* = \frac{\kappa U_0}{\ln\left(\frac{z}{z_0}\right)}$$

$L_1 = 8.1 * \Lambda_1$

$$\Lambda_1 = \begin{cases} 0.7z & z \le 60\ m \\ 42 & z > 60\ m \end{cases}$$

z = turbine hub height [m]

z_0 = surface roughness length [m]

f = frequency [Hz]

The duration of each simulated interval of high-rate turbulence must be $2T_{sample,input}$ in order to generate frequency content up to $f_{Nyq,input}$, the highest frequency that the input data can resolve according to the Sampling Theorem [12]. Each simulated period will contain $N = 2T_{sample,\ input}\ f_{output}$ points; if N is not an integer, we round it up to the nearest even integer.

Each simulated time series corresponds to two low-rate measurements, so we must combine the measured means U_0 and variances σ_u^2 according to the following formulas:

$$U_0(p \bigcup p+1) = \frac{(U_0(p)\ T_{s,i}(p) + U_0(p+1)\ T_{s,i}(p+1))}{T_{s,i}(p) + T_{s,i}(p+1)} = \frac{U_0(p) + U_0(p+1)}{2} \qquad (3)$$

$$\sigma_u^2(p \bigcup p+1) = \sqrt{\frac{\sigma_u^2(p)\ T_{s,i}(p) + \sigma_u^2(p+1)\ T_{s,i}(p+1)}{T_{s,i}(p) + T_{s,i}(p+1)} + \frac{T_{s,i}(p)\ T_{s,i}(p+1)}{T_{s,i}(p) + T_{s,i}(p+1)} (U_0(p) - U_0(p+1))^2} \qquad (4)$$

where we use the abbreviation $T_{s,I} = T_{sample,input}$.

We discretize the continuous one-sided Kaimal spectrum $S(f)$ in equation (1) or (2) at discrete frequencies $f_m = m\Delta f$:

$$\mathbf{S}[m] = S(f_m)\,\Delta f \quad m = \{0,\ 1,\ \ldots,\ M-1\} \qquad (5)$$

There are $M = 1 + N/2$ unique frequencies in the one-sided spectrum, where $N = 2T_{sample,\ input} f_{output}$. We require that N be an even integer, so M will be an odd integer based on the definition above. We force $S[0] = 0$ because the steady-state ("DC") value of the simulated data is zero because we are simulating a zero-mean process.

We scale the magnitude of the discretized spectrum according to the following formula:

$$\mathbf{V}[m] = \sqrt{\tfrac{1}{2}\eta\,\mathbf{S}[m]}\ e^{i\,\phi[m]} \qquad (6)$$

The term $e^{i\phi[m]}$ creates random phases in $\mathbf{V}$ that make the output of Veers method random. The phases $e^{i\phi[m]}$ are complex numbers and $S[m]$ are real numbers, so $\mathbf{V}[m]$ are complex numbers. The phase angles $\phi[m]$ are drawn from a uniform random distribution over the range [0 2π]. Nearly all simulations that use the Shinozuka/Veers method use uniform randomly-distributed phase angles. Shinozuka proves that a simulated time series will be ergodic if uniform randomly-distributed phase angles are used [16]. In our analysis of measured wind speed data sampled at 5 – 52 Hz, we found that the differences between adjacent phase angles can be described by a von Mises distribution [17] and that the fit of the von Mises distribution improves for higher sampling frequencies. However, we find that it is statistically impossible to distinguish between uniform and von Mises distributions for the sampling frequencies used in our paper (~1 Hz). The dispersion parameter κ of the phase differences, analogous to the standard deviation in a normal distribution, is so low at this sampling frequency that statistical tests cannot establish that a von Mises distribution fits the data.

The factor of 1/2 in equation (6) is necessary because we will create a two-sided spectrum from **V**, but the spectra in equations (1) and (2) are one-sided spectra. The factor of ½ should be omitted if a two-sided spectrum is used. We introduce η to normalize $S[m]$ to compensate for the variance lost when $S(f)$ is discretized.

The factor η accounts for the difference between the desired variance $\sigma^2_{desired}$ and the actual variance σ^2_{actual} of data simulated with the discretized spectrum in equation (5). We define η as:

$$\eta = \frac{\sigma^2_{desired}}{\int_{\Delta f - \frac{1}{2}\Delta f}^{\Delta f + \frac{1}{2}\Delta f} S(f)df} \quad (7)$$

In theory, the variance σ^2 of wind turbulence simulated from a one-sided spectrum is given by equation (8) and approximated by (9), assuming that M is large:

$$\sigma^2 = \int_0^\infty S(f)df \quad (8)$$

$$\approx \sum_{m=0}^{M} S[m] \quad (9)$$

In practice, the actual variance of the simulated wind turbulence is smaller than predicted in (8) and (9) because $S[0] = 0$ and M is not infinite. This is a problem because variance is a parameter in the spectrum in equation (1) and we want the variance of the simulated turbulence output to equal that parameter.

We show in Figure 2 that the actual variance of the simulated turbulence output is well-predicted by the following formula:

$$\sigma^2_{actual} \approx \sum_{m=1}^{M} S[m] \approx \int_{\Delta f - \frac{1}{2}\Delta f}^{f_{max} + \frac{1}{2}\Delta f} s(f)df \quad (10)$$

where the integration limits in (10) are determined by the method for discretizing the continuous spectrum, best illustrated by figure 1 in a paper by Yang [18]. The integral of the continuous spectrum in a small region around f_m is approximated by a rectangle of height $S[m]$ and width Δf:

$$S[m]\Delta f = \int_{f_m - \frac{1}{2}\Delta f}^{f_m + \frac{1}{2}\Delta f} S(f)df \quad (11)$$

Figure 2 shows that discretizing the turbulence spectrum causes a loss of variance in the simulated turbulence. We simulated 400 – 1600 seconds of turbulence at sampling frequencies from 0.2 – 20 Hz using Veers method and the Kaimal spectrum in equation (1). The actual variance of simulated turbulence deviates significantly from the desired variance ($\sigma^2_{desired} = 1$); the actual variance only approaches the desired variance asymptotically with increasing sampling frequency ($f_{output} \to \infty$) and increasing sample period ($T \to \infty$). In this paper, we use a sampling frequency of 5 Hz and a sampling period of 1200 sec; that means the variance of each period of simulated turbulence is approximately 8% lower than the measured variance used as a parameter in the simulation.

We correct for that loss of variance using equation (10). Equation (10) (dotted lines) closely predicts the actual variance of simulated turbulence (solid lines) without running a simulation. We use that prediction to calculate η in equation (7), and use η in equation (6) to scale the spectrum so the variance of the simulated turbulence measured the desired variance.

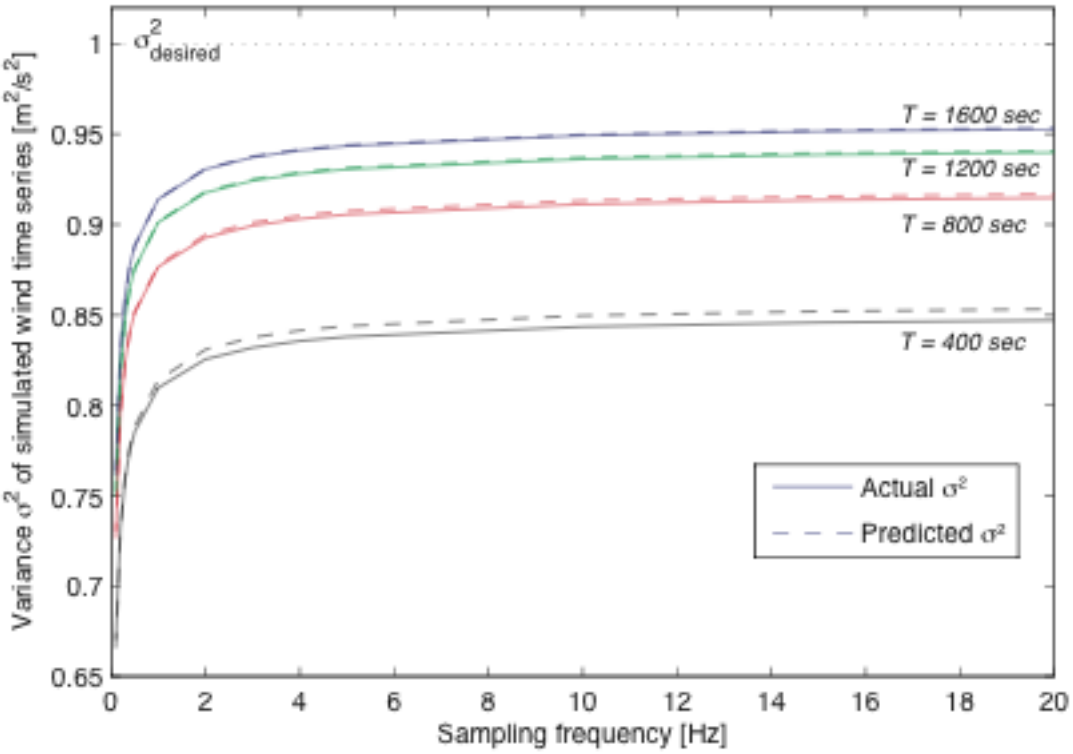

Figure 2: This figure plots the actual variance of turbulence simulated with the Kaimal spectrum in equation (1) and a variance parameter $\sigma^2_{desired}$ = 1 against the sampling frequency of the simulation. Different curves plot simulations of different lengths. The actual variance is plotted as solid lines and the variance predicted by equation (10) is plotted as dotted lines. The turbulence is simulated with Veers method, the Kaimal spectrum from equation (1), U_0 = 10 m/s, $\sigma^2_{desired}$ = 1 m²/s², and z = 65 m.

We use the following pattern to create a two-sided spectrum of N points:

$$\mathbf{V}_{2\,side} = [0,\ \mathbf{V}[2],\ \mathbf{V}[3],\ \ldots,\ \mathbf{V}[M-1],\ |\mathbf{V}[M]|\,,\ \mathbf{V}^*[M-1],\ \ldots,\ \mathbf{V}^*[2]] \qquad (12)$$

where the negative frequencies are represented in the second half of $\mathbf{V}_{2\,side}$, each $\mathbf{V}_{2\,side}[n]$ is complex-valued except $\mathbf{V}_{2\,side}[N/2]$, and the first element $\mathbf{V}_{2\,side}[1]$ is forced to zero because we are creating a zero-mean simulation. To produce a time series of real-valued wind speeds, the $\mathbf{V}_{2\,side}$ must be conjugate symmetric, i.e. $\mathbf{V}_{2\,side}[n] = \mathbf{V}^*_{2\,side}[\mathrm{mod}(N-n+1,\ N)+1]$, where the * operator represents complex conjugation. Note that the magnitudes of the one-sided spectra in equations (1) or (2) are multiplied by 1/2 in equation (6) in anticipation of creating the two-sided spectrum in equation (12).

We calculate the turbulence time series output **u** using the Fast Fourier Transform (FFT):

$$\mathbf{u} = |\mathrm{FFT}(\mathbf{V}_{2\,side})| \qquad (13)$$

where the FFT is defined following Press [12] as:

$$\mathbf{u}[n] = \sum_{k=1}^{N} \mathbf{V}_{2\,side}[k] e^{i2\pi(n-1)(k-1)/N} \quad n = \{1, \ldots, N\} \qquad (14)$$

In theory it is not necessary to take the absolute value of the FFT in equation (13) because the conjugate-symmetric two-sided spectrum we constructed in equation (12) ensures the output of the FFT will be real-valued. In practice, the limited numerical precision of computers may cause the output $u[n]$ to have small imaginary values.

Confusingly, different sources define the Fast Fourier Transform (FFT) and its inverse in opposite ways. Press [12] gives the definition of the FFT in equation (14), but Bracewell [19] and Newland [20] define that as the inverse FFT. The Matlab software uses the definition in equation (14) except for a minus sign in the exponential term; Mathematica accepts a parameter for the choice of definitions.

2.3. Combining Empirical and Simulated Data (D)

We create the hybrid wind speed time series by concatenating the blocks of simulated zero-mean turbulence and superimposing them on the filtered measured mean data (Figure 1D). We find that windowing the periods of simulated turbulence suggested by some authors [6,10] is not necessary. We do not encounter the problem of excessive spectral content at low frequencies noted by McFarlane [6] because our method does not overlap consecutive blocks of simulated high-frequency data and because we low-pass filter the measured data,

2.4. Extension to Three Dimensions

We do not consider the general three-dimensional case of the Veers method here; good explanations can be found in papers by Veers [5] and Sørensen [21], but we will briefly summarize how to extend the one-dimensional case described above. A simulated 3-D wind field consists of parallel, coherent 1-D wind speed time series. A coherence matrix γ is introduced in equation (6), so the discretized spectrum $\mathbf{S}[m]$ must be a square matrix Because $\mathbf{S}[m]$ is a square matrix, the square root operation must be replaced by the Cholesky decomposition or similar decomposition that yields a lower-triangular matrix. Similarly, the random phases in the $e^{i\phi[m]}$ term of equation (6) must be replaced by a square matrix with complex random phase angles on the diagonal and zeros elsewhere.

2.5. Application Notes

The method we present here can be used to generate wind speed time series data for many applications that require higher frequency data than is available. However, certain applications require details we have not discussed above.

Power production: The large rotors on multi-megawatt wind turbines filter most high-frequency turbulence, but make the power output of those turbines sensitive to the significant wind speed differences across the rotor induced by shear. Wagner has shown that calculating the power performance of a wind turbine from only hub-height wind speed measurements introduces significant uncertainties [22]; related research by Antoniou has shown hub-height measurements introduce similar uncertainties in power curve and wind resource calculation [23]. Wagner proposes several methods to calculate an "equivalent" wind speed that better account for wind shear and better model power production [22]. Dolan proposes an alternative formula to calculate an equivalent wind speed based on a wind shear function [24]. These methods calculate an equivalent wind speed from wind speeds measured at several heights within the area of the turbine rotor. Our hybrid method can be used to generate wind speed times series at multiple heights, but the results will be sensitive to the models of wind shear and vertical coherence used. We also recommend simulating the low-pass filtering effect of the large rotor with the $H_{\psi,0}(s)$ filter proposed by Sørensen [3].

Power quality/Flicker: Power quality and flicker analyses deal with power variations at frequencies higher than approximately 1 Hz [25]. The large rotor of multi-megawatt wind turbines filters most wind fluctuations at frequencies higher than 10^{-1} Hz [26], but wind shear and the aerodynamic effect of blades passing the tower introduces noise at three times the

rotation frequency ("3p"). We recommend applying the $H_{\psi,0}(s)$ and $H_{\psi,3}(s)$ filters proposed by Sørensen [3] to simulate the low-pass filtering effect of the large rotor and the 3p effect of wind shear and blades passing the tower. Careful attention should be paid to modeling the generator and oscillation modes of the blades, drivetrain, and tower, although those topics are beyond the scope of the method we propose for simulating wind speed.

Mechanical Load Simulation: Mechanical load simulations typically require high-frequency wind speed data over the three-dimensional wind field. We recommend extending our proposed method to three dimensions, as outlined above in section 2.4. We also recommend applying the $H_{\psi,0}(s)$ and $H_{\psi,3}(s)$ filters proposed by Sørensen [3] to simulate the low-pass filtering effect of the large rotor and the effect of blades passing the tower, and applying a model of vertical wind shear to simulate the unbalanced wind load on the rotor.

3. Validation

We validate the method for creating hybrid wind speed data described above by comparing the data it generates to wind speed data measured at three sites in the U.S. The hybrid method was created to support simulations of wind power variability on time scales relevant to grid frequency regulation, so we focus on validating the characteristics of the hybrid method that are most important for that application. First we compare the characteristics of wind speed variation, especially the Power Spectral Density (PSD). Then we use that wind speed data to drive a simulated wind turbine to create wind power data. We compare the energy production and ramp rate characteristics of the wind power over different time scales.

The procedure for creating the data used to validate the hybrid wind method is:

1. Collect measured wind speed data from field measurements (see Table 1) and decimate data to 5 Hz.
    a. The measured 5 Hz data are the "Measured" data set
2. Calculate 10-minute statistics (mean and standard deviation) from measured wind data in step 1.
    a. The measured 10-minute mean wind speeds (resampled to 5 Hz) are the "Measured, 10-min avg" data set
3. Generate 5 Hz hybrid wind speed data
    a. Hybrid data created with equation (1), which takes wind speed standard deviation as an input, are the "Hybrid, σ" data set
    b. Hybrid data created with equation (2), which takes estimated surface roughness length as an input, are the "Hybrid, z_0" data set
4. Generate wind power data by simulating a 2-MW wind turbine driven by wind speed from the data sets created in steps 1a, 2a, 3a, and 3b.

Figure 3 and Figure 4 compare the wind speed data from steps 1 – 3 above. Figure 5 - Figure 8 compare the wind power data from step 4.

3.1. Validation Data

To validate our hybrid method of creating long wind speed time series, we used publically-available wind speed data from three experiments conducted by the U.S. National Center for Atmospheric Research (NCAR): CASES99 (Cooperative Atmosphere-Surface Exchange Study) [27,28], FLOSSII (Fluxes Over Snow Surfaces, Phase II) [29,30], and ATST (Advanced

Technology Solar Telescope site survey) [30,31], summarized in Table 1. We decimate these data to 5 Hz by low-pass filtering and then down-sampling the data, and then calculate the along-wind horizontal (longitudinal) wind speed. The large rotor on modern wind turbines acts as a low-pass filter to attenuate phenomena faster than approximately 0.5 Hz [26], so we choose a sampling rate of 5 Hz to ensure we capture all significant power variations.

Table 1: Properties of data sets from three U.S. National Center for Atmospheric Research (NCAR) experiments used to validate the hybrid wind model.

Data Set Name	Location	Measurement Height	Sampling Frequency	Surface Roughness Length z_0 (estimated)	Dates Sampled
CASES99	Leon, Kansas	55 m	20 Hz	0.03 m	6 – 30 Oct., 1999
FLOSSII	North Park, Colorado	30 m	60 Hz	0.03 m	20 – 31 Nov., 2002 15 – 29 Dec., 2002
ATST	Big Bear Lake, California	25 m	30 Hz	0.003 m	7 May – 14 June, 2004

We group the data into contiguous blocks that share common atmospheric stability properties. First we calculate the stability criterion value $1/L$ for each 1-hour period, where L is the Obukhov length from Businger [30] calculated according to equation (15) below. Next we determine the Pasquill atmospheric stability class [31] corresponding to the calculated value of $1/L$ using a nomogram given by Golder [32], assuming the roughness lengths z_0 given in Table 1. Finally, we create each block of data by selecting the contiguous data with the same stability class: stable (Pasquill A, B, C), neutral (Pasquill D), or unstable (Pasquill E, F) and require that each block of data be a minimum of 2 hours long. The distribution of the data in the stability classes is shown in Table 2.

$$L = \frac{u_*^3 \overline{T}}{\kappa\, g\, \overline{w' T_v'}} \qquad (15)$$

where

$u_* = \left(\overline{u'w'}^2 + \overline{v'w'}^2 \right)^{1/4}$ = friction velocity (definition from Weber [33])

u = along-wind velocity
v = across-wind velocity
w = vertical wind velocity
T = absolute temperature
T_v = virtual temperature
$\kappa = 0.4$ = von Kármán constant
$g = 9.8$ m/s^2 = acceleration of gravity
$\overline{a'b'}$ = covariance of two variables a and b

Table 2: Distribution of the measured wind speed data in different atmospheric stability classes

Data Set	Stable Data [hours]	Neutral Data [hours]	Unstable Data [hours]
CASES99	148	177	10
FLOSSII	111	150	0
ATST	46	87	111

3.2. Wind Speed Time Series

Figure 3 qualitatively compares wind speed time series generated with our hybrid method to a measured wind speed time series. The two hybrid wind speed data sets ("Hybrid, σ" and "Hybrid, z_0") are generated by calculating the 10-minute mean and variance of the measured time series, then superimposing simulated high-frequency turbulence. The "Measured, 10-min avg." plot shows the kind of measured data commonly captured from meteorological masts that would be used as the basis for generating hybrid wind data.

The plots in Figure 3 demonstrate that the hybrid method generates realistic non-stationary wind speed data. The hybrid wind data accurately model doubling of the wind speed, from t = 2000 to t = 4000, and doubling of the variance, from t = 7000 to t = 10000.

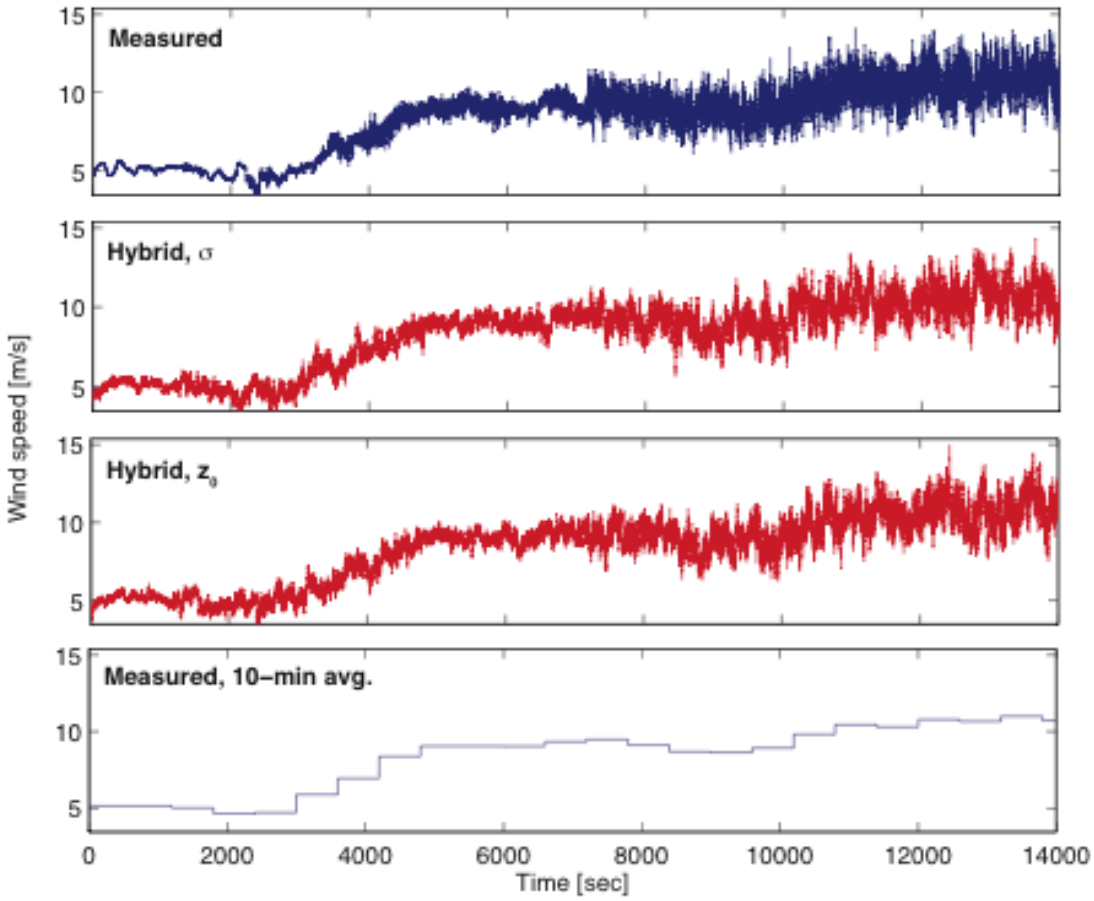

Figure 3: A comparison of measured wind speed data ("Measured"), hybrid wind speed data generated with empirical mean and variance statistics ("Hybrid, σ"), hybrid wind speed data generated with empirical mean statistics and

estimated surface roughness length ("Hybrid, z_0"), and empirical mean statistics ("Measured, 10-min avg."). These dataare representative of the close match between hybrid wind speed data and measured data with similar statistical properties. These plots show 4 hours of data from the CASES99 experiment beginning at 20:00:00 October 28, 1999 (stable atmospheric conditions). The hybrid and "Measured, 10-min avg." data is generated using 10-minute statistics derived from the "Measured" data.

3.3. Wind Turbulence Spectra

We compare the PSD (Power Spectral Density) of hybrid wind speed time series to the PSD of measured wind speed time series from the CASES99 experiment. We calculate the PSD according to the following formula:

$$S_{2\ side}(f) = T\left|\mathrm{FFT}^{-1}(\mathbf{u})\right|^2 \qquad (16)$$

where T is the duration of the data in second and the inverse Fourier Transform is defined by Press [12] as:

$$\mathbf{V}_{2\ side}[k] = \frac{1}{N}\sum_{n=1}^{N}\mathbf{u}[n]e^{-i2\pi(n-1)(k-1)/N} \quad k = \{1,\ldots,N\} \qquad (17)$$

Each PSD plotted in Figure 4 is the average of all the PSDs of 2-hour periods with the mean wind speed between 6 and 8 m/s. This averaging, called "segment averaging" by Press [12] reduces the variance of the PSD. The number of periods averaged is given in the title of each plot. We plot the spectra for mean wind speeds 6 – 8 m/s to because that range consistently contains the most data across the three experimental sites. We plot the spectra of four different data sets: "Measured" is ATST field data decimated to 5 Hz, "Hybrid, σ" is hybrid data created with the Kaimal spectral model in equation (1), "Hybrid, z0" is hybrid data created with the Kaimal spectral model in equation (2), and "Measured, 10-min avg" is 10-minute means of the ATST field data. Hybrid wind is essentially simulated turbulence superimposed on the "Measured, 10-min avg" data, so this last data set shows the results if the hybrid method is not used.

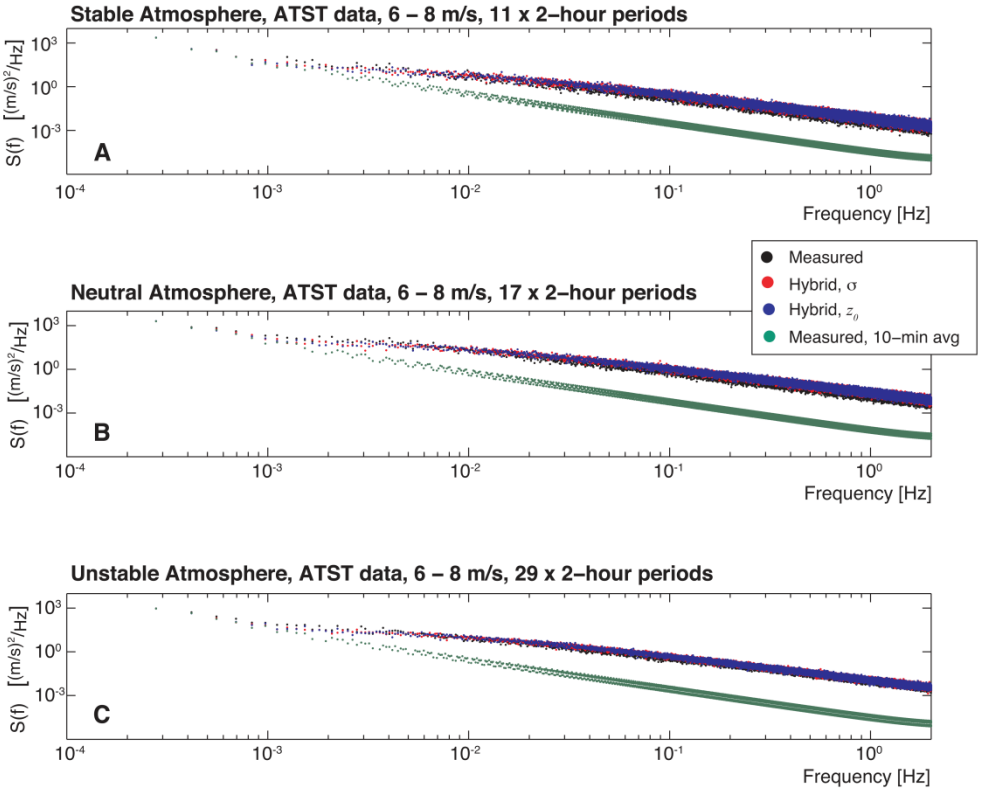

Figure 4: A comparison of Power Spectral Densities (PSD) of measured wind data, both variants of hybrid wind speed data, and measured 10-minute average data from the ATST field site for 6 – 8 m/s mean wind speed. Each PSD is the segment average of the PSDs all 2-hour segments of data in the specified mean wind speed range (see description in text). Data from stable conditions (0.01 < 1/L < 0.15) are plotted in (A), neutral conditions (-0.03 < 1/L < 0.01) are plotted in (B), and unstable conditions (-0.15 1/L < -0.03) in (C). We plot the spectral only to 2 Hz because we decimate (low-pass filter and down-sample) the measured data to 5 Hz, but the low-pass filtering attenuates the spectra of the measured data above 2 Hz.

The spectra of the hybrid wind data in Figure 4 closely match the spectra of the measured ATST wind data in stable, neutral, and unstable atmospheric conditions. The spectra of wind speed data generated with both hybrid variants is almost indistinguishable from the spectra of the measured data at all frequencies. These results are representative of the results for other range of mean wind speed and for data from the CASES99 and FLOSSII experiments with one exception: the hybrid wind under-predicts the magnitude of turbulence for frequencies in the range of 1 x 10^{-3} – 3 x 10^{-3} Hz when compared to data from the CASES99 test site during stable atmospheric conditions. That range of frequencies is where measured data is joined with simulated turbulence to form hybrid wind, which suggests that the low-pass filter applied in Step C of the hybrid method may not be steep enough. However, this under-prediction is not evident in neutral and unstable CASES99 data or in any of the ATST and FLOSSII data.

The spectra of the 10-min average data matches (plotted in green) very poorly with spectra of the measured data; we expect this result because the 10-min average data should contain almost no frequency content at frequencies higher than 1.7 x 10^{-3} Hz, the frequency corresponding to 10

minutes. The poor fit of the spectra of 10-minute average data demonstrates the advantage of the hybrid method: the hybrid method adds the turbulence the 10-minute average data lacks.

3.4. Wind Turbine Simulation Model

All wind power data used in this paper are created by simulating the output of a single 2-MW wind turbine with different measured and hybrid wind inputs. The turbine is pitch-regulated, variable speed turbine with an 80-m rotor, modeled using the Wind Turbine Blockset, v3.0 developed by Aalborg University [34]. The turbine design parameters, control scheme, control parameters, and first-order generator model are those recommended by the Danish Technical University (DTU) [35]. We incorporate a rotor-wind filter $H_{\psi,0}(s)$ proposed by Sørensen [3] into the wind turbine model to simulate the filtering effect of a large rotor on turbulence that is not spatially homogeneous, but we do not account for the effect of vertical wind shear across the rotor disk.

3.5. Validation of Power Production

We compare the energy and power produced by one 2-MW wind turbine with 40-meter blades (described in Section 3.4) fed with both the measured and hybrid wind speed time series. Comparing simulated wind power takes into account the filtering effect of a large wind turbine on wind speed fluctuations and the dynamic response of a modern turbine to those fluctuations. We do not compare simulated wind power to wind power measured from actual wind turbines because of the difficulties in controlling the output of actual turbines for wind direction, wakes, terrain, mechanical and electrical losses, power limits, and ramp rate limits. Future work should analyze met-mast and wind power data to give a more thorough comparison of the hybrid method to the output of an actual wind turbine.

Figure 5 shows a comparison between the energy generated by a 2MW wind turbine driven by the measured wind data described in Table 1 and the corresponding hybrid wind data. Each sub-plot shows the percent error in energy generation in 1-hour periods. Figure 5A compares hybrid wind data generated using equation (1), which takes wind speed standard deviation as a parameter. Figure 5B compares hybrid wind data generated using equation (2), which takes surface roughness length as a parameter. Figure 5C compares measures 10-minute average wind data to show the results if the hybrid method is not used to fill in high-frequency turbulence.

We define the 1-hour percent energy generation error ϵ in hour k as:

$$\epsilon(k) = \frac{E_{emp}(k) - E_{hyb}(k)}{E_{emp}(k)} \qquad (18)$$

where $E_{emp}(k)$ is the energy generated by the simulated wind turbine driven by measured wind data in hour k and $E_{hyb}(k)$ is the energy generated with hybrid wind data in hour k.

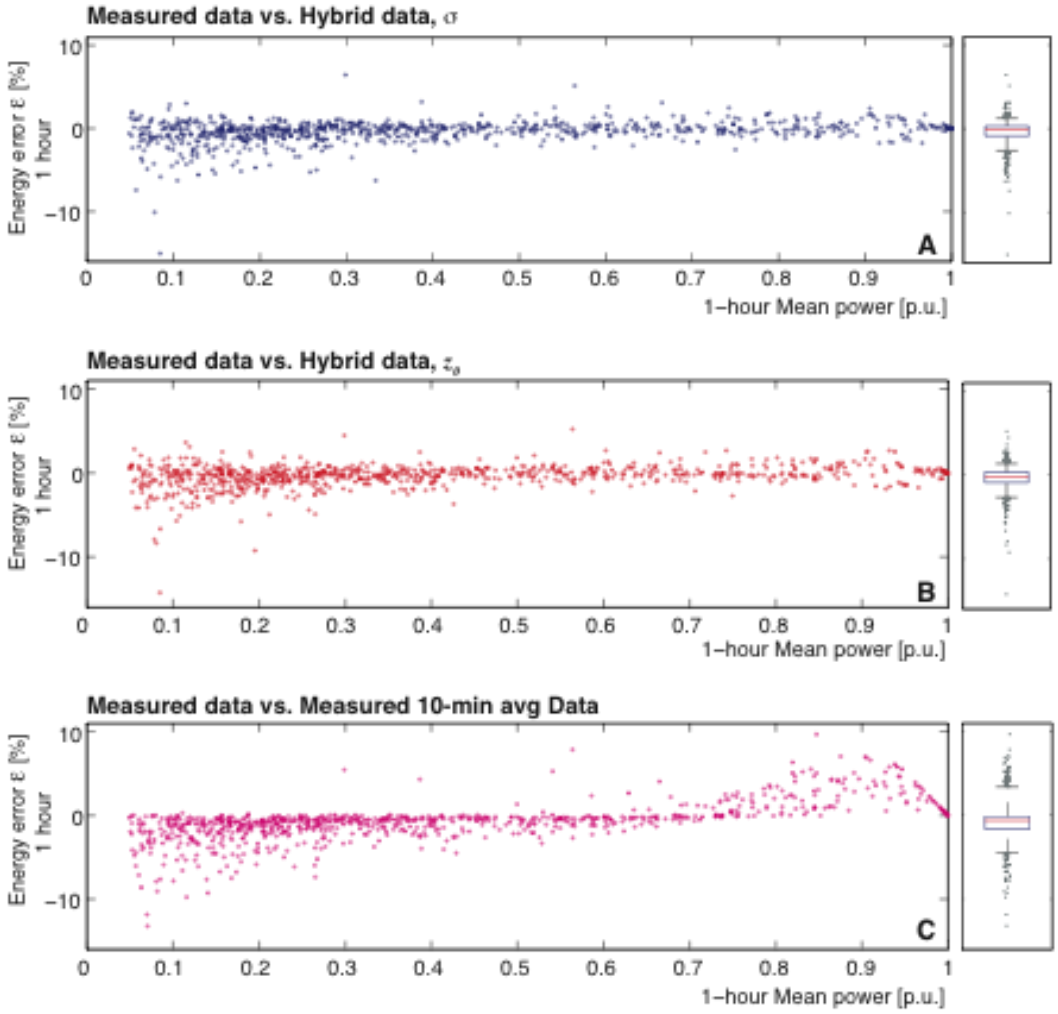

Figure 5: The plots on the left show percent difference in energy production ε between a turbine simulated with empirical wind data and hybrid wind data, plotted against per-unit (p.u.) mean power. (A) compares measured data to hybrid data created with equation (1), (B) compares measured data to hybrid data created with equation (2), and (C) compares measured data to 10-minute average measured data. The boxplots on the right plot the mean (center line), 25th and 75th percentile values (bottom and top of box), and the 5th and 95th percentiles (bottom and top "whiskers") of the same data [36].

Figure 5 shows both variants of hybrid wind (Figure 5A and B) have smaller errors in energy production than the 10-minute average data (Figure 5C) they are based on. The mean error for hybrid data created with both methods (A and B) is -0.4%; the mean error for the 10-minute average data (C) is -0.8%. Hybrid data also gives significantly less variance in the errors: 90% of the hybrid errors fall between -2.7% and +1.4%, whereas 90% of the errors for the 10-minute average data fall between -4.5% and 3.4%. Using the hybrid method to add high-frequency turbulence to low-frequency measured data significantly reduces the magnitude and range of error in energy production. The hybrid method also reduces the trend of energy error increasing as a function of mean power: Figure 5C shows that using 10-minute average data over-predicts energy production when the average power is low and under-predicts energy when the average power is high. Data created with the hybrid method do not show such a strong trend.

3.5.1. Power Ramp Rate

Figure 6 and Figure 7 show comparisons of the ramp rates of power generated by a 2-MW wind turbine driven by the measured wind data described in Table 1 to the corresponding hybrid wind data. Validation of the ramp rates is important to confirm that the hybrid method accurately models the variations on different time scales. Figure 6 shows a comparison of the distribution of sizes of ramp events and Figure 7 compares the size of extreme ramp events.

We use the definition that the ramp rate is the change in mean power from one period to the next: $P_{ramp}(n) = P_{mean}(n+1) - P_{mean}(n)$ [9]. The ramp rates are binned by the mean power of the starting period $P_{mean}(n)$. We analyze ramp rates over three different time scales: 10 minutes, 1 minute, and 10 seconds. The 10-minute ramp rates correspond to phenomena in the "load-following" time scale, 1-minute ramp rates correspond to phenomena in the "frequency-regulation" time scale, and the 10-second ramp rates correspond to "flicker" phenomena.

The duration curves in Figure 6 plot the percentile values of ramp rates. Ramp events are grouped together in bins by initial power $P_{mean}(n)$; Figure 6 shows the duration curves for 10-minute, 1-minute, and 10-second ramp events with an initial power of 0.6 to 0.7 per-unit (p.u.). This figure is similar to comparisons of measured and simulated wind power ramp rates given by Brower for validation of the Eastern Wind Integration and Transmission Study, but we plot a cumulative distribution function (CDF) where Brower plots a probability density function (PDF) [40].

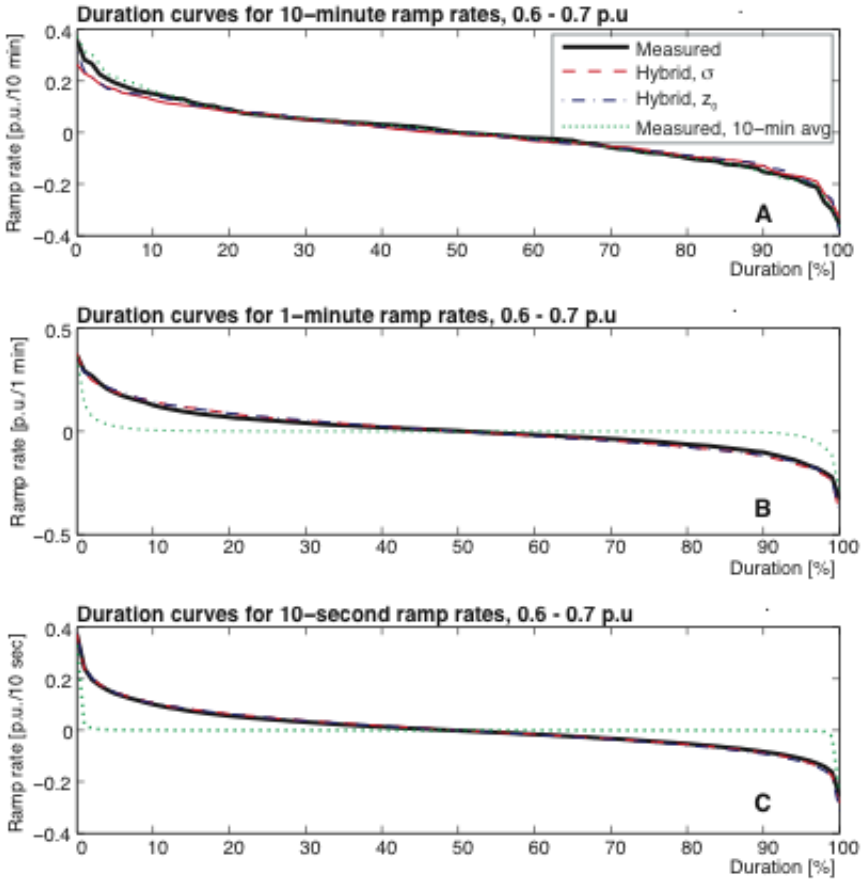

Figure 6: A comparison of the distribution (percentiles) of power ramp rates for a simulated turbine driven by measured and hybrid wind data. All plots show changes in power starting in the range 0.6 – 0.7 per-unit (p.u.); (A) shows the distribution of 10-minute ramp rates, (B) the distribution of 1-minute ramp rates, and (C) the distribution of 10-second ramp rates. The hybrid data are nearly indistinguishable from the measured data, especially for 1-minute and 10-second ramp rates.

Figure 6 shows that the hybrid methods are slightly worse at modeling 10-minute ramp rates than 10-minute average measured data (A), but much better at modeling 1-minute and 10-second ramp rates (B and C). For 10-minute ramp rates starting from the 0.6 – 0.7 p.u. power range (Figure 6A), the mean-square error (MSE) between the measured data and the 10-minute average measured data is 0.87×10^{-4} p.u./10-min, significantly smaller than MSEs for the two hybrid data sets: 3.3×10^{-4} p.u./10-min and 2.2×10^{-4} p.u./10-min. For 1-minute ramp rates (Figure 6B), the MSE for the hybrid data sets is 1.9×10^{-4} p.u./1-min but the MSE for the 10-minute average measured data is more than an order of magnitude larger: 59×10^{-4} p.u./1-min. For 10-second ramp rates (Figure 6C), the MSEs for the hybrid data sets are 3.0×10^{-5} and 6.7×10^{-5} p.u./10-sec but the MSE for the 10-minute average measured data is two orders of magnitude larger: 490×10^{-5} p.u./10-sec. These results are typical of the results in all other initial power ranges.

The power ramp rates based on hybrid wind data match very closely to the power ramp rates based on measured wind over time scales from 10 minutes to 10 seconds. The good match between hybrid and measured ramp rates on these time scales shows that the simulated turbulence introduced by the hybrid method models the characteristics of actual wind turbulence well. It is somewhat surprising that the hybrid wind predicts10-minute power ramps that are smaller than than10-minute average measured data because the hybrid method adds zero-mean turbulence that should not affect the 10-minute ramp rate. We suspect that the under-prediction of 10-minute ramp rates by the hybrid method is an artifact of the low-pass filter used in creating the hybrid data. Figure 4 supports this hypothesis—the spectra of hybrid wind diverge slightly from the spectra of measured wind at approximately 1.1×10^{-3} Hz, which corresponds to a period of ~15 minutes.

Figure 7 plots the 1st percentile (most extreme down ramps) 10-minute, 1-minute, and 10-second ramp rates as a function of initial power $P_{mean}(n)$. The data are grouped by initial power into 0.1 p.u. bins, so each plotted point is the 1st percentile ramp rate value for all the data in a particular bin. These plots are a cross-sectional slice of the plots in Figure 6, but varying the initial power instead of the percentile value. The 1st percentile ramp rates are significant because they put the greatest burden on other generators to compensate for the decrease in wind power.

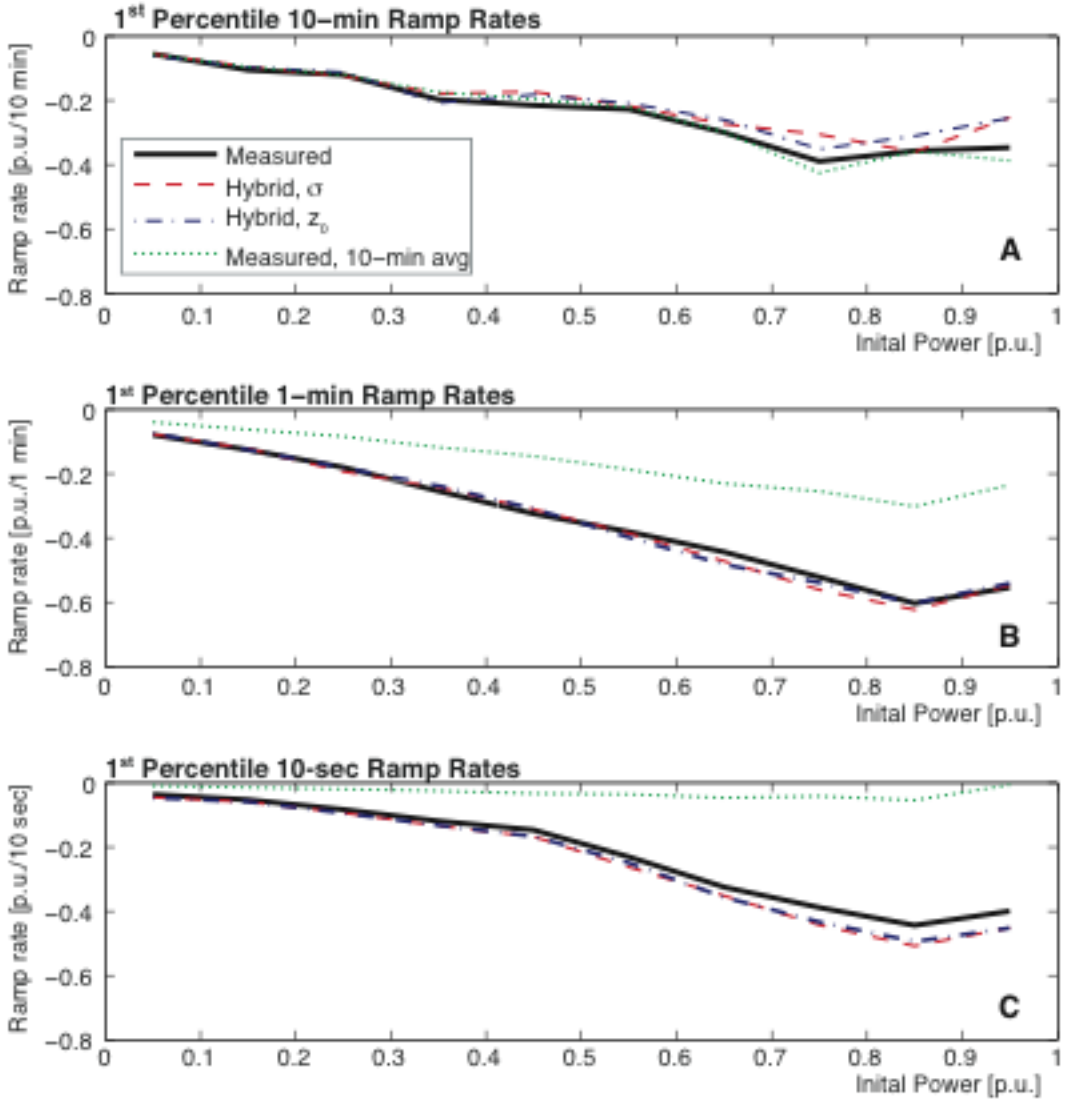

Figure 7: The extreme (1st percentile) power ramp rates for a simulated turbine driven by measured and hybrid wind data. Each plot shows the extreme power down ramp as a function of the initial power (power output at the start of ramping). (A) shows the distribution of extreme 10-minute ramp rates, (B) the distribution of extreme 1-minute ramp rates, and (C) the distribution of extreme 10-second ramp rates. The ramp rates of the hybrid data closely match the ramp rates of the measured data, but the hybrid data predicts more extreme 10-second ramp rates for initial power output in the range 0.7 – 1 p.u.

The data for extreme power ramp rates plotted in Figure 7 show a similar trend to the data in Figure 6: the hybrid data model power ramps over short periods (1-minute and 10-seconds) better than the 10-minute average data, but slightly worse for 10-minute ramping periods. For the 1st percentile 10-minute ramp rates (Figure 7A), the mean-square error (MSE) between the measured data and the 10-minute average measured data is 0.40×10^{-3} p.u./10-min, significantly smaller than the MSEs for the two hybrid data sets: 1.9×10^{-3} p.u./10-min and 1.5×10^{-4} p.u./10-min. For the 1st percentile 1-minute ramp rates (Figure 7B), the 10-minute average measured data

has a MSE of 1000 x 10^{-5} p.u./1-min, several orders of magnitude larger than the MSEs of the hybrid data: 8.2 x 10^{-5} and 6.9 x 10^{-5} p.u./1-min. Similarly for the 1st percentile 10-second ramp rates (Figure 7C), the 10-minute average measured data has a MSE of 140 x 10^{-4} p.u./1-min compared to the MSEs of the hybrid data: 3.1 x 10^{-4} and 2.4 x 10^{-4} p.u./10-sec.

Similar to the ramp rate duration curves in Figure 6, the 1st percentile power ramp rates based on hybrid wind data match very closely to the power ramp rates based on measured wind over time scales from 10 minutes to 10 seconds. They do not match as well on a time scale of 10 minutes—we suspect that the under-prediction of 10-minute ramp rates by the hybrid method is an artifact of the low-pass filter used in creating the hybrid data. However, we are surprised that the hybrid data sets diverge significantly at higher initial powers. The hybrid method under-predicts extreme down ramp rates by 2.5% of the rated turbine power output (0.025 p.u.) for initial power 0.8 – 0.9 p.u., suggesting that the hybrid method generates too much turbulence at higher wind speeds.

3.6. Validation of Spinning Reserve Requirements

Figure 8 compares the power reserves needed for power generated by a 2MW wind turbine driven by the measured wind data described in Table 1 and the corresponding hybrid wind data. Validation of the power reserve requirements is important to confirm that the hybrid method accurately models the variations on different time scale. We define the reserve requirement as the difference between mean power in one period and minimum power in the next: $P_{ramp}(n) = P_{mean}(n) - P_{min}(n+1)$ [9]. The reserve requirement values are binned by the mean power of the starting period $P_{mean}(n)$. As we did for the ramp rates, we analyze reserve requirements on 10-minute, 1-minute, and 10-second time scales. We analyze the 99th percentile reserve requirements because these represent the most extreme reserve requirements.

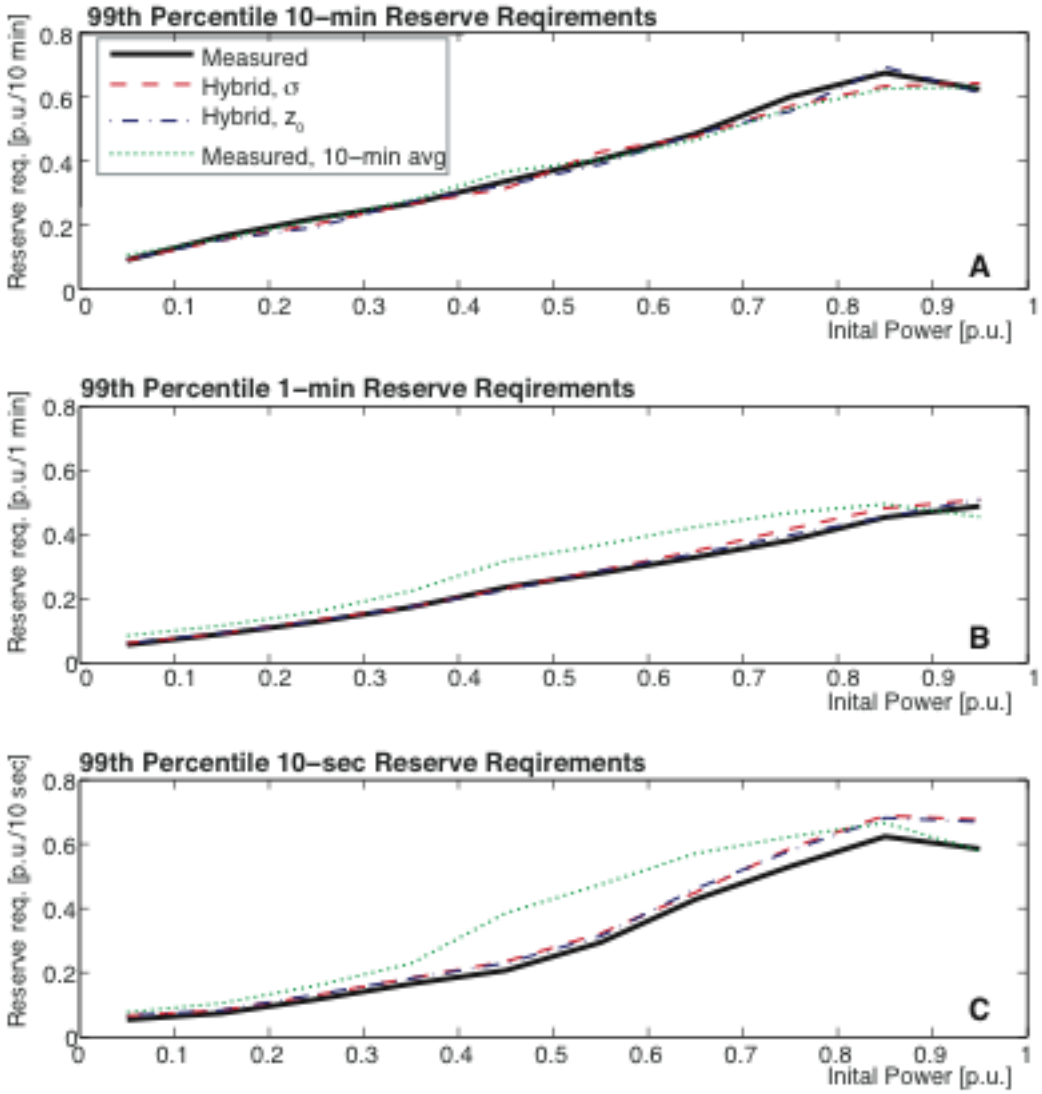

Figure 8: The extreme (99st percentile) reserve requirements for a simulated turbine driven by measured and hybrid wind data. Each plot shows the extreme reserve requirement as a function of the initial power (power output at the start of ramping). (A) shows the distribution of extreme 10-minute reserves, (B) the distribution of extreme 1-minute reserves, and (C) the distribution of extreme 10-second reserves. The reserve requirements of the hybrid data closely match the reserve requirements of the measured data, but the hybrid data predicts more extreme 10-second reserve requirements for initial power output in the range 0.7 – 1 p.u.

The data for extreme power reserve requirements plotted in Figure 8 show that the hybrid method is consistently better at predicting reserve requirements than the 10-minute average measured data. For 10-minute reserve requirements (Figure 8A), the 10-minute average data is nearly as good as the hybrid data: it has a MSE of 4.5 x 10^{-4} p.u. compared to the MSEs of the hybrid data of 3.8 x 10^{-4} and 4.5 x 10^{-4} p.u. For 1-minute reserve requirements (Figure 8B), the hybrid method is significantly better: the MSE for 10-minute average data is 38 x 10^{-4} p.u., an order of magnitude worse than the MSEs for the hybrid data: 3.0 x 10^{-4} and 0.97 x 10^{-4} p.u. For 10-second reserve requirements (Figure 8C), the MSE for the 10-minute average data is 26 x 10^{-4} p.u. and the MSEs for the hybrid data are 4.6 x 10^{-4} and 3.9 x 10^{-4} p.u.

As with the extreme ramp rates in Figure 7, the hybrid data sets diverge significantly at higher initial powers. The hybrid method over-predicts extreme reserve requirements by 3% of

rated turbine power output (0.03 pu.u) for initial power 0.8 – 0.9 p.u. This suggests that the hybrid method generates too much wind turbulence at higher wind speeds.

4. Conclusions

We demonstrate a method for creating long wind speed time series as a hybrid of measured and simulated wind speed. This method is meant to take advantage of wind speed data measured at low frequencies by meteorological stations and wind farm developers, and data simulated with appropriate spatial and temporal resolution by meso-scale weather models. The measured wind data captures non-stationary phenomena such as diurnal variations, the passing of weather systems, and seasonal variations, while our hybrid method simulates data to interpolate the fast turbulent variations that are needed to accurately model fast variations in wind power.

Our analysis shows that the wind speed time series created with our hybrid method accurately reproduce measured wind speed data from three different sites and in neutral, stable, and unstable atmospheres. We demonstrate that the total energy produced by a wind turbine simulated with hybrid wind is within -2.7%/+1.5% of the energy produced by the same turbine simulated with measured wind data for 90% of the tested period. We also demonstrate that the power ramp rates and spinning reserve requirements for a turbine simulated with hybrid wind data very closely match the results for a turbine simulated with measured wind data.

This method is well suited to studies of the fluctuations of wind farm power on the scale of seconds to minutes. It generates wind speed data time series sampled fast enough to simulate dynamic behavior of individual wind turbines, such as pitch control, but retains their time-dependent characteristics such as diurnal variations, the passing of weather fronts, and seasonal variations.

5. Works Cited

1 National Oceanic and Atmospheric Administration. Automated Surface Observing System (ASOS) User's Guide. [Internet]. 1998 [cited 2010 October 11]. Available from: http://www.nws.noaa.gov/asos/aum-toc.pdf.

2 Kareem A. Numerical Simulation of Wind Effects: A Probabilistic Perspective. 2008;96(10-11):1472-1479. DOI: 10.1016/j.jweia.2008.02.048

3 Sørensen P, Hansen AD, Rosas PAC. Wind models for simulation of power fluctuations from wind farms. Journal of Wind Engineering & Industrial Aerodynamics. 2002 1381-1402. DOI: 10.1016/S0167-6105(02)00260-X

4 Nichita C, Luca D, Dakyo B, Ceanga E. Large Band Simulation of the Wind Speed for Real Time Wind Turbine Simulators. IEEE Transactions on Energy Conversion. 2002;17(4):523-529. DOI: 10.1109/TEC.2002.805216

5 Veers PS. Modeling Stochastic Wind Loads on Vertical Axis Wind Turbines. SAND83-1909. 1984.

6 McFarlane A, Veers PS, Schluter L. Simulating high-frequency wind for long durations. In: 13th ASME Wind Energy Symposium; 1994 Jan 1; New Orleans. Available from: http://www.osti.gov/energycitations/product.biblio.jsp?osti_id=10193698.

7 Kelly ND, Sutherland HJ. Damage Estimates from Long-Term Structureal Analysis of a

Wind Turbine in a U.S. Wind Farm Environment. In: 16th ASME/AIAA Wind Energy Symposium; 1997; Reno.

8 Negra NB, Holmstrøm O, Bak-Jensen B, Sørensen P. Model of a Synthetic Wind Speed Time Series Generator. Wind Energy. 2008;11:193-209. DOI: 10.1002/we.244

9 Sørensen P, Cutululis NA, Antonio VR, Jensen LF, Hjerrild J, Donovan MH, Madsen H. Power Fluctutations from Large Wind Farms. IEEE Transactions on Power Systems. 2007;22(3):958-965. DOI: 10.1109/TPWRS.2007.901615

10 Smallwood DO, Paez TL. A frequency domain method for the generation of partially coherent normal stationary time domain signals. Shock and Vibration. 1993;1(1):45-53.

11 Nielsen M, Larsen GC, Hansen KS. Simulation of Inhomogeneous, Non-Stationary and Non-Gaussian Turbulent Winds. Journal of Physics: Conference Series. 2007;75. DOI: 10.1088/1742-6596/75/1/012060

12 Press WH, Teukolsky SA, Vetterling WT, Flannery BP. Numerical Recipes 3rd Edition: The Art of Scientific Computing. 2007.

13 Kaimal JC, Wyngaard JC, Izumi Y, Coté OR. Spectral Characteristics of Surface-Layer Turbulence. Quarterly Journal of the Royal Meteorological Society. 1972;98:563-589.

14 International Electrotechnical Commission. IEC 61400-1: Wind Turbines- Part 1: Design requirements (3rd Edition). IEC; 2005. 61400-1.

15 Shinozuka M, Jan CM. Digital simulation of random processes and its applications. Journal of Sound and Vibration. 1972;25(1):111 - 128. DOI: 10.1016/0022-460X(72)90600-1

16 Shinozuka M, Deodatis G. Simulation of stochastic processes by spectral representation. Applied Mechanics Reviews. 1991;44(4):191 - 203. DOI: 10.1115/1.3119501

17 Fisher NI. Statistical Analysis of Circular Data. Cambridge University Press; 1996.

18 Yang JN. On the Normality and Accuracy of Simulated Random Processes. Journal of Sound and Vibration. 1973;26(3):417 - 428. DOI: 10.1016/S0022-460X(73)80196-8

19 Bracewell RN. The Fourier Transform and Its Applications. McGraw-Hill; 2000.

20 Newland DE. An Introduction to Random Vibrations and Spectral Analysis. Longman; 1975.

21 Sørensen P, Cutululis NA, Vigueras-Rodríguez A, Madsen H, Pinson P, Jensen LE, Hjerrild J, Donovan M. Modelling of Power Fluctuations from Large Offshore Wind Farms. Wind Energy. 2008;11(1):29 - 43. DOI: 10.1002/we.246

22 Wagner R, Antoniou I, Pedersen SM, Courtney MS, Jørgensen HE. The Influence of the Wind Speed Profile on Wind Turbine Performance Measurements. Wind Energy. 2009;12(4):348-362. DOI: 10.1002/we.297

23 Antoniou I, Pedersen SM, Enevoldsen PB. Wind Shear and Uncertainties in Power Curve Measurement and Wind Resources. Wind Engineering. 2009;33(5):449-468. DOI: 10.1260/030952409790291208

24 Dolan DSL, Lehn PW. Simulation Model of Wind Turbine 3p Torque Oscillations due to Wind Shear and Tower Shadow. IEEE Transactions on Energy Conversion. 2006;21(3):717-724. DOI: 10.1109/TEC.2006.874211

25 Moreno CV, Duarte HA, Garcia JU. Propagation of Flicker in Electric Power Networks Due to Wind Energy Conversion Systems. IEEE Transactions on Energy Conversion.

2002;17(2):267-272. DOI: 10.1109/TEC.2002.1009479

26 Apt J. The Spectrum of Power from Wind Turbines. Journal of Power Sources. 2007;169(2):369-374. DOI: 10.1016/j.jpowsour.2007.02.077

27 Oncley S. The Integrated Surface Flux Facility during CASES99. [Internet]. [cited 2010 Mar 8]. Available from: http://www.eol.ucar.edu/isf/projects/CASES99/isff.shtml.

28 Poulos GS, Blumen W, Fritts DC, Lundquist JK, Sun J, Burns SP, Nappo C, Banta R, Newsom R, Cuxarat J, et al. CASES-99: A comprehensive investigation of the stable nocturnal boundary layer. Bulletin of the American Meteorological Societ. 2002;83(4):555-581. DOI: 10.1175/1520-0477(2002)083<0555:CACIOT>2.3.CO;2

29 Oncley S. Fluxes Over Snow Surfaces, Phase II. [Internet]. [cited 2010 Apr 24]. Available from: http://www.eol.ucar.edu/isf/projects/FLOSSII/.

30 Mahrt L, Vickers D. Boundary-Layer Adjustment Over Small-Scale Changes of Surface Heat Flux. Boundary-Layer Meteorology. 2005;116(2):313-330. DOI: 10.1007/s10546-004-1669-z

31 Maclean G, Oncley S. ATST Site Survey Report. [Internet]. [cited 2010 Apr 21]. Available from: http://www.eol.ucar.edu/isf/projects/ATST/.

32 Socas-Navarro H, Beckers J, Brandt P, Briggs J, Brown T, Brown W, Collados M, Denker C, Fletcher S, Hegwer S, et al. Solar Site Survey for the Advanced Technology Solar Telescope. I. Analysis of Seeing Data. Publications of the Astronomical Society of the Pacific. 2005;117:1296-1305. DOI: 10.1086/496939

33 Businger JA. A note on the Businger-Dyer profiles. Boundary-Layer Meteorology. 1988;42(1):145-151.

34 Pasquill F. Atmospheric Diffusion. London: Van Nostrand; 1962.

35 Golder D. Relations Among Stability Parameters in the Surface Layer. Bourdary-Layer Meteorology. 1972;3(1):47-58.

36 Weber RO. Remarks on the Definition and Estimation of Friction Velocity. Boundary-Layer Meteorology. 1999;93(2):197 -205. DOI: 10.1023/A:1002043826623

37 Iov F, Hansen AD, Sørensen P, Blaabjerg F. Wind Turbine Blockset in Matlab/Simulink. Aalborg University; 2004. 87-89179-46-3.

38 Hansen MH, Hansen AD, Larsen TJ, Øye S, Sørensen P, Fuglsang P. Control design for a pitch-regulated, variable speed wind turbine. Risø National Laboratory; 2005 Feb 1. Risø-R-1500(EN).

39 McGill R, Tukey J, Larsen W. Variations of box plots. American Statistician. 1978;32(1):12-16.

40 Brower M. Development of Easern Regional Wind Resource and Wind Plant Output Datasetes. Albany: AWS Truewind, LLC; 2009. NREL/SR-550-46764.

Acknowledgments

The authors thank Mitch Small for his advice on statistical methods. This work was supported in part by a grant from the Alfred P. Sloan Foundation and EPRI to the Carnegie Mellon Electricity Industry Center, the Doris Duke Charitable Foundation, the Department of Energy National

Energy Technology Laboratory, and the Heinz Endowments for support of the RenewElec program at Carnegie Mellon University. This research was also supported through the Climate and Energy Decision Making (CEDM) center funded under NSF grant SES-0949710 to Carnegie Mellon University.